Title: Genome-wide association study of pericardial fat area in 28,161 UK Biobank participants

Authors:
Ahmed Salih (Queen Mary University of London)
Maddalena Ardissino (Imperial College London)
Aaron Wagen
Andrew Bard (Queen Mary University of London)
Liliana Szabo (The William Harvey Research Institute)
Mina Ryten (University College London)
Steffen Petersen (Queen Mary University of London)
Andre Altmann (University College London)
Zahra Raisi-Estabragh (The William Harvey Research Institute)

Genome-wide association study of pericardial fat area in 28,161 UK Biobank participants

Ahmed Salih*[1], Maddalena Ardissino*[2,3], Aaron Z. Wagen[4,5,6], Andrew Bard[1], Liliana Szabo[1,7,8], Mina Ryten[4,9], Steffen E. Petersen[1,7,10,11], André Altmann †[12], Zahra Raisi-Estabragh †[1,7]

* co-first authors with equal contribution

† co-senior authors with equal contribution

1. William Harvey Research Institute, NIHR Barts Biomedical Research Centre, Queen Mary University of London, Charterhouse Square, London, EC1M 6BQ, UK
2. National Heart and Lung Institute, Imperial College London, London, W12 0HS, UK
3. Heart and Lung Research Institute, University of Cambridge, Cambridge, CB2 0AY
4. Genetics and Genomic Medicine, Great Ormond Street Institute of Child Health, University College London, London, UK
5. Department of Clinical and Movement Neurosciences, Queen Square Institute of Neurology, London, UK
6. Neurodegeneration Biology Laboratory, The Francis Crick Institute, London, UK
7. Barts Heart Centre, St Bartholomew's Hospital, Barts Health NHS Trust, West Smithfield, London, EC1A 7BE, UK
8. Semmelweis University, Heart and Vascular Center, Budapest Hungary
9. NIHR Great Ormond Street Hospital Biomedical Research Centre, University College London, London, UK
10. Health Data Research UK, London, UK
11. Alan Turing Institute, London, UK
12. Centre for Medical Image Computing (CMIC), Department of Medical Physics and Biomedical Engineering, University College London, London, United Kingdom

Corresponding author:

Dr Ahmed Salih; William Harvey Research Institute, NIHR Barts Biomedical Research Centre

Queen Mary University of London, Charterhouse Square, London, EC1M 6BQ

Telephone: +44 7442 334388

E-mail:a.salih@qmul.ac.uk

Abstract

Background: Pericardial adipose tissue (PAT) is the visceral adipose tissue compartment surrounding the heart. Experimental and observational research has suggested that greater PAT deposition might mediate cardiovascular disease, independent of general or subcutaneous adiposity. We characterize the genetic architecture of adiposity-adjusted PAT and identify causal associations between PAT and adverse cardiac magnetic resonance imaging (CMR) measures of cardiac structure and function in 28,161 UK Biobank participants.

Methods: The PAT phenotype was extracted from CMR images of using an automated image analysis tool previously developed and validated in this cohort. A genome wide association study was performed with PAT area set as the phenotype, adjusting for age, sex, and other measures of obesity. Functional mapping and Bayesian Colocalisation were used to understand biologic role of identified variants. Mendelian Randomization analysis was used to examine potential causal links between genetically-determined PAT and CMR-derived measured of left ventricular structure and function.

Results: We discovered 12 genome-wide significant variants, with two independent sentinel variants (rs6428792, p= 4.20×10^{-8} and rs11992444, p= 1.30×10^{-12}) at two distinct genomic loci, that were mapped to three potentially causal genes (TBX15, WARS2, EBF2) through functional annotation. Bayesian colocalization additionally suggested a role of RP4-712E4.1. Genetically-predicted differences in adiposity-adjusted PAT were causally associated with adverse left ventricular remodelling.

Conclusion: This study provides insights into the genetic architecture determining differential PAT deposition, identifies causal links with left structural and functional parameters, and provides novel data regarding the pathophysiological importance of adiposity distribution.

Clinical Perspective

What is new?

- This study identifies multiple distinct genetic loci associated with pericardial fat area, after accounting for multiple measures of whole-body adiposity
- Mendelian randomization analyses identified an association of likely causal relevance of genetically-predicted pericardial fat with adverse cardiac structural and functional parameters

What are the clinical implications?

- In addition to being determined by whole-body adiposity this study suggests that the proportional deposition of pericardial adipose tissue is, to an extent, genetically determined
- A greater genetically-predicted pericardial adipose tissue is linked with markers of adverse left cardiac structure and function, suggesting a role in determining adverse left ventricular remodelling

Introduction

Pericardial adipose tissue (PAT) is the visceral adipose tissue compartment surrounding the heart. Experimental research has suggested that a proportionally greater deposition of PAT might mediate risk of cardiovascular disease in addition to that conferred by general adiposity, through paracrine proinflammatory effects of the fat tissue on adjacent myocardium and coronary arteries[1–4]. In line with this, observational studies have reported associations between PAT and risk of coronary artery disease[5], heart failure[6] atrial fibrillation[7,8], and adverse imaging markers of cardiac structure and function[9,10] even after adjustment for multiple measures of general adiposity and its visceral and subcutaneous tissue distribution.

Body fat distribution is a highly heritable trait, with twin-based estimates for body mass index (BMI)-adjusted waist:hip ratio (WHR) estimated between 30-60%[11], and SNP-based heritability in the region of 20-50%[12]. So far, BMI-adjusted WHR[13] has been the main focus of large-scale studies exploring genetic determinants of fat distribution. Consequently, the genetic architecture and disease consequences of this trait have been thoroughly explored[14–17]. On the other hand, current understanding of the genetic determinants of fat deposition specifically in the pericardial tissue, independent of general adiposity and its distribution, remains limited.

At present, only two genome-wide association studies (GWAS) have evaluated genetic determinants of PAT in relation to whole-body adiposity[18,19]. The largest of these, carried out in 2017 by Chu *et al*, included 18,332 participants and discovered three genetic variants in distinct loci associated with PAT after height and weight adjustment: rs6587515 in *ENSA*, rs1650505 in *EBF1*, and rs10198628 in *TRIB2*. Genetic discovery in this field has been limited by the lack of large-scale data. We recently developed a fully automated, quality-controlled tool for PAT quantification from cardiac magnetic resonance (CMR) images[20], enabling extraction of PAT measurements in 42,598 participants in the UK Biobank, a large-scale cohort study collecting clinical, genetic, imaging and laboratory data from participants throughout the United Kingdom.

In this study, we employed UK Biobank data to investigate the genetic variants predisposing to deposition of PAT independent of other measures of total adiposity and its distribution. We additionally leverage these variants to assess the causal role of PAT on left ventricular structure and function.

Methods

Data access and availability

This study was conducted using the UK Biobank under application 2964. The work is covered by ethical approval from the National Health Service (NHS) National Research Ethics Service on 17th June 2011 (Ref 11/NW/0382) and extended on 18 June 2021 (Ref 21/NW/0157). Written, informed consent was obtained from all participants.

The data produced from this study, including summary statistics, methods, and materials will be returned to the UK Biobank. These will become available to all bona fide researchers for the purpose of health-related research under approved applications, without preferential or exclusive access. Further details regarding application and access procedures are available at the UK Biobank website (http://www.ukbiobank.ac.uk/ register-apply/).

Study population

The UK Biobank is a population-based cohort study based in the United Kingdom. Over 500,000 participants aged 40-69 years were recruited between 2006-2010, and underwent a baseline assessment and regular integration of health outcomes through healthcare record linkage. The detailed study protocol is publicly available[21]. The UK Biobank Imaging Study is an ongoing subset of the UK Biobank, aiming to perform multiorgan magnetic resonance imaging (MRI) of the heart, brain, and abdomen in a randomly selected 20% (n=100,000) subset of UK Biobank participants.

Pericardial fat quantification

CMR scans were performed using 1.5 Tesla scanners (MAGNETOM Aera, Syngo Platform VD13A, Siemens Healthcare, Erlangen, Germany) in specific imaging units. Scanning was performed according to pre-defined protocols[22]. PAT area was extracted from CMR 4-chamber cine images in end-diastole using an automated tool that has been developed and validated in the UK Biobank and an external cohort[20]. This involves a neural network trained to perform fully automated PAT segmentation through a multi-residual U-net architecture. It

includes an in-built quality-control feature, which uses Dice scores as a measure of segmentation quality that was used to select scans with good segmentation (Dice score >0.7). In the study population, PAT areas had a right-skewed distribution, and were therefore log-transformed for linear modelling.

Measures of adiposity

A key aim of the study was to determine whether the relationship between PAT and cardiovascular phenotypes was distinct from other obesity measures. We considered anthropometric measures of obesity, impedance fat measures, and abdominal MRI derived measures of visceral and subcutaneous adiposity. BMI and WHR were calculated from UK Biobank body size measures. Bioelectrical impedance measures of obesity were derived using the Tanita BC418MA body composition analyzer as per UK Biobank protocols[23]. We included whole body fat mass and trunk fat mass impedance measures. From abdominal MRI (available for 15,518 participants), we selected abdominal subcutaneous, visceral adipose tissue, and total adipose tissue volume measures, which are only available for a subset of participants[24].

Genetic data and quality control

Genotyping was performed in all consenting individuals. Genotypes were directly called using the two closely related arrays UK Biobank Axiom (Affymetrix, Santa Clara, California) and UK BiLEVE Axiom. Imputation was carried out using the Haplotype Reference Consortium and UK10K + 1000Genomes (Phase 3) reference panels.

Genome-wide association study

For genome-wide association analysis, participants were excluded if their genetic samples failed bioinformatic quality control (missing rate on autosomes of >0.2 or mismatch between reported and genetically inferred sex), if they were related (based on a kinship matrix with threshold K>0.175) by excluding one of the pair. The cohort was restricted to European ancestry. After exclusion criteria were applied, 28,161 participants were included. Among the

159 available imputed and genotyped variants, we restricted the analysis to autosomal variants
160 with a MAF>0.01 and imputation quality score (INFO sore) >0.3. This resulted in an
161 approximate 9,283,970 million variants. Genome-wide association analysis was performed
162 using PLINK[25] and BOLT-LMM[26].

163 In the main model, we assessed the association between variants and PAT after adjusting for
164 sex, age, age^2, age*sex, 10 genetic principal components (PCs), assessment centre, genotype
165 array, BMI, WHR, whole body fat mass, trunk fat mass and body fat percentage. In this
166 analysis, principal component analysis (PCA) was applied to BMI, WHR, whole body fat
167 mass, trunk fat mass and body fat percentage to explain at least 90% of the variance, which
168 resulted in 2 PCs that explained 99% of the variance in the included phenotypes. These two
169 PCs were included when GWAS was run instead of the BMI, WHR, whole body fat mass,
170 trunk fat mass and body fat percentage. For this model the population was randomly split into
171 set of 18,774 participants for discovery and a replication set of 9,387 participants for
172 replication. This is the primary analysis of the study.

173 For discovery analysis, the threshold for statistical significance was considered $p<5x10^{-8}$ to
174 account for multiple tests. Replication analyses were carried out for all genome-wide
175 significant variant associations in the primary model. For replication analysis, the statistical
176 significance threshold was calculated using Bonferroni correction based on the number of
177 variants tested for validation ($p<0.05/n$; where n = number of lead variants to validate).

178 To increase the power to detect significant signal using the whole sample, we additionally
179 performed a meta-analysis GWAS by combining the GWAS summary statistics of the
180 discovery and replication. The analysis was conducted using Metal tool[27].

181 We have also carried out a more relaxed GWAS without adjustment for different fat
182 measures. The analysis was adjusted for sex, age, age^2, age * sex, 10 genetic PCs, assessment
183 center and genotype array.

184 **Functional annotation**

Functional mapping was carried out using Functional Mapping and Annotation of GWAS (FUMA) v1.5.0[28]. Independent significant SNPs were defined as those associated with PAT in the primary discovery analysis model with $p<5x10^{-8}$ that were correlated with $r^2<0.6$. Additional candidate SNPs were identified by extracting SNPs in LD with these at $r^2>0.6$ using the 1000Genomes Phase 3 European reference panel[29]. Finally, lead SNPs were identified among the candidates as the uncorrelated ($r^2<0.1$) SNPs with prioritization of those with lowest p-value for the association with PAT. For lead SNPs and any SNPs in LD with these at $r^2>0.8$, all reported phenotypic associations were listed using GWASCatalog[30].

The functional consequences of the candidate SNPs on genes were determined using ANNOVAR[31]. Deleteriousness score was described using CADD scores (with score > 12.37 considered likely deleterious)[32], and SNPs were annotated for regulatory functions using RegulomeDB score[33], for 15-core chromatin state using ChromHMM[34,35], tissue-specific eQTLs[36], and for 3D chromatin interactions using Hi-C data[37].

Gene mapping was performed using positional, eQTL and chromatin interactions mapping. First, genomic risk loci near independent significant SNPs were outlined using a maximum distance of 10kB. Within each risk locus, the SNP with the lowest p-value was defined as the lead SNP for the locus. Probability of loss of function intolerance was annotated using pLI scores for coding genes[38], and with non-coding residual variation intolerance scores (ncRVIS) for non-coding genes[39]. MAGMA gene-based analysis was performed to assess the association between protein coding genes and PAT[40]. Since the input SNPs were mapped to 19,086 protein coding genes, genome wide significance for this analysis was Bonferroni corrected at p-value = $0.05/19{,}086 = 2.620x10^{-6}$. Tissue-specific eQTL mapping was then performed using data from single cell RNA sequencing (scRNA)[41] in immune cells, and Genotype-Tissue Expression (GTEx) Project v8[36] tissue-specific eQTL data for arterial, adipose and cardiac tissues. Finally, chromatin mapping was performed using tissue-specific chromatin interaction (Hi-C) data for the aorta, left ventricle and right ventricle[37,42–44].

To understand putative biological mechanisms behind mapped genes, gene to function mapping was performed within FUMA and GWASAtlas. GTEx v8[36] data was utilized to visualize normalized tissue specific expression patterns for each gene. Differentially expressed gene set (DEG) analyses were performed to test for differential expression of mapped genes across tissue types. Finally, phenome-wide associations were identified for all potentially causal genes using GWASAtlas[45]. Finally, the International Mouse Phenotyping Consortium (IMPC) database was searched for information regarding previous mouse models for potentially causal genes[46].

Colocalisation analysis

To evaluate the probability that GWAS loci and expression quantitative trait loci (eQTLs) share a single causal variant, a colocalisation analysis was performed using coloc (v5.1.0.1) and colochelpR (version 0.99.1)[47,48]. Cis-eQTLs were derived from GTEx v8[36,49]. GWAS loci within 1 Mb of the 11 significant GWAS SNPs were explored. Loci identified through chromatin mapping were not included as these were expected to have trans-associations. Associations were explored in seven GTEx tissues: aortic artery (N = 387), coronary artery (N = 213), tibial artery (N = 584), subcutaneous adipose (N = 581), visceral adipose (N = 469), the cardiac atrial appendage (N = 372) and the cardiac left ventricle (N = 386). The prior probability that any random SNP in the region is associated with the GWAS (p_1) or eQTL (p_2), was set to the default 10^{-4}, while the prior probability that any random SNP in the region is associated with both traits (p_{12}) was set to 10^{-5}. A posterior probability of hypothesis 4 (PPH4) measures the probability that a locus is colocalised due to a single causal variant, as opposed to two distinct causal variants (PPH3). A PPH4 $\geq$ 0.8 was considered significant. All colocalizations were subjected to sensitivity analyses using coloc's sensitivity() function, which plots prior and posterior probabilities of each coloc hypothesis as a function of the p12 prior. This permits exploration of the robustness of results to changes in the p12 prior. Code for coloc analyses is openly available at

https://github.com/aaronwagen/Pericardial_fat_gwas_coloc/.

Heritability and genetic associations

We used CTG-VL 0.5 beta (https://vl-dev.genoma.io/updates) to estimate trait heritability and calculate genetic correlation between PAT and multiple disease phenotypes. These included adiposity traits (trunk fat mass as percentage, whole body fat mass), cardiovascular risk factors (hypertension, diabetes, obesity), and cardiovascular outcomes (coronary heart disease, coronary event, heart failure, stroke, atrial fibrillation and flutter, and cardiac death).

Mendelian randomization (MR) was performed to assess the causal relevance of PAT on multiple cardiovascular magnetic resonance (CMR) markers of left ventricular (LV) structure and function, motivated by the previously established observational evidence suggesting potential causal mechanisms[9]. Genome-wide significant ($p<5x10^{-8}$), uncorrelated ($r^2<0.001$) variants for PAT were selected as instrumental variants. Instrument strength was quantified using F-statistics. Gene-outcome association data was extracted from summary statistics of Pirruccello *et al*'s GWAS on 45,504 UK Biobank participants[50] for indexed left ventricular end diastolic volume (LVEDV), left ventricular end systolic volume (LVESV), left ventricular stroke volume (LVSV), and left ventricular ejection fraction (LVEF). Additional gene-outcome association data was extracted from Aung *et al*'s GWAS on 16,923 participants for left ventricular mass (LVM) and mass to end diastolic volume ratio (LVM:LVEDV)[51]. Inverse-variance weighted MR with fixed effects was utilized for primary analysis. Single-SNP analysis was performed using the Wald ratio method. Importantly, the data sources for both gene-exposure and gene-outcome association estimates in this case is the UK Biobank cohort. Though the MR methods utilized are considered 'two-sample' methods, they have been demonstrated to be robust for individual-level analysis when applied in the setting of large-scale biobanks[52]. All MR analyses were performed using the MendelianRandomization package (version 0.7.0) [53] in RStudio (R version 4.1.2)[54].

Results

Genome-wide association study

Genetic variants associated with pericardial fat independent of body mass index and other fat distribution measures

We used previously validated, automated, and quality-controlled tool to extract measures of PAT area in 28,161 UKB participants, who were randomly split into a discovery set of 18,774 participants, and a testing set of 9,387 participants.

In the genome-wide association analysis in the discovery set, and after adjusting for sex, age, age^2, age*sex, 10 genetic principal components (PCs), assessment centre, genotype array, and 2 PCs reflecting BMI, WHR, whole body fat mass, trunk fat mass, body fat percentage, a total of 11 genome-wide significant variants were identified (rs11992444, rs6428792, rs10923752, rs10923748, rs6428794, rs12036872, rs4304634, rs764891110, rs4659150, rs4659146, rs2885227) as reported in **Supplementary Figure 1, Supplementary Table 1** and **Table 1**. The QQ plot for the results is presented in **Supplementary Figure 2**. Genomic inflation factor (lambda, λ) was 1.026, and λ1000 was 1.001.

Among the discovered variants, one single variant was located on chromosome 8, rs11992444 ($p = 5.10x10^{-13}$) and ten variants were located on chromosome 1, among which the variant with lowest p-value was rs6428792 ($p = 7.40x10^{-9}$). The association of all 11 genome-wide significant variants with PAT was replicated in the replication set at the Bonferroni-corrected p-value threshold ($p<0.0045$), as reported in **Table 2**.

Functional annotation

Functional annotation through positional, eQTL and chromatin interaction mapping identified a total of 10 potentially causal genes. A visual representation of the annotation process and key results are provided in **Figure 1**.

Positional mapping

In addition to the 11 GWAS-tagged variants, one additional closely correlated variant (rs72707349) was extracted using the 1000 genomes reference panel. Among the 12 candidate SNPs, two lead variants were identified (r^2<0.1): rs6428792 and rs11992444, in two separate genetic loci (**Supp Tables 1-3**). All previously reported phenotypic associations for these two SNPs and SNPs in close LD with these (r^2>0.8) are reported in **Supp Table 4**, these included multiple BMI-adjusted adiposity traits, body shape indices, and lipid traits.

Among the 12 candidate variants, the 11 variants on Chromosome 1 were intronic (of which one in non-coding RNA), and the variant on Chromosome 8 was intergenic (**Supp Table 5**). RegulomeDB score for both variants was 7, indicating a lack of evidence regarding potential regulatory functions. The minimum 15-core chromatin state was 5 for rs6428792, indicating weak transcription function, and 7 for rs11992444, indicating enhancer chromatin state. Positional mapping prioritized three genes: *WARS2* (protein coding), *RPS3AP12* (pseudogenic) and *RP11-418J17.1* (antisense), all mapped to the Chromosome 1 locus (**Supp Table 6**). Among these, *WARS2* had the highest maximum SNP CADD score of 10.56; and the remaining two had low risk of deleteriousness (CADD 6.85 for *RPS3AP12*, and CADD 3.06 for *RP11-418J17.1*). The nearest genes for the chromosome 8 risk locus were *CDCA2* and *RP11-219J21.1*, though these were distant, respectively 99,254 and 78,624 bases from the risk locus (**Supp Table 5**).

eQTL mapping

eQTL mapping consistently prioritized *WARS2* (protein coding, expressed in adipose, arterial, and cardiac tissues) and *RP11-418J17.1* (antisense, expressed in adipose, arterial, and cardiac tissues); but additionally identified regulatory functions of the candidate variants on *TBX15* (protein coding, expressed in adipose tissues), and *RP4-712E4.1* (lincRNA, expressed in adipose and arterial tissue) (**Supp Table 6, Supp Table 7**). No Chromosome 8 genes were mapped using eQTLs. The locus plots, positional mapping and corresponding eQTLs for Chromosome 1 variants are summarized in **Figure 2**. Notably, the *TBX15* gene was also

highlighted as the most strongly associated protein-coding gene with adjusted PAT in MAGMA genome-wide analysis (**Supplementary Figure 3**).

Chromatin interaction mapping

Finally, 11 chromatin interaction regions were identified (**Supp Table 8**) mapping to 5 distinct genes (**Supp Table 6**). These are depicted in **Figure 3** and **Figure 4**. Using chromatin interaction mapping, a total of 3 genes were mapped in Chromosome 8: *EBF2*, *AC090103.1* and *SDAD1P1*. Among these, the protein coding *EBF2* gene appeared highly intolerant to loss of function (pLI 0.97).

Colocalisation analysis

Colocalisation analysis was performed to explore whether risk variants for PAT were associated with gene expression in adipose, arterial and cardiac tissues. Utilising cis-eQTLs from GTEx v8, associations were explored within 1 Mb of significant GWAS SNPs. In the discovery GWAS, evidence for colocalisation was found in the *RP4-712E4.1* locus in subcutaneous adipose tissue (PPH4 = 0.93) and tibial artery (PPH4 = 0.96, **Supp Table 9**, **Supplementary Figure** 4, 5). For SNPs in the region surrounding *RP4-712E4.1*, PAT risk and *RP4-712E4.1* tended to correlate, suggesting that increased PAT risk is associated with increased *RP4-712E4.1* expression (**Supplementary Figure** 4-D, 5-D). These results were not duplicated in the replication dataset. Sensitivity analysis confirmed that these colocalisations were robust to changes in the prior probability of a variant associating with both traits (i.e., p_{12} prior, **Supplementary Figure** 6). An additional locus of high PPH4 was found between the gene *CDCA2* in the left ventricle, in both discovery and replication datasets, although these were driven by a single SNP (**Supplementary Figure** 7). Multiple associations were found for loci where SNPs independently associated with PAT risk and gene expression in a region, including the *DOCK5* locus using the tibial artery eQTL (PPH3 = 0.93 in discovery and replication datasets), and in the *WARS2* and *RP11-418J17.1* loci in all seven tissues tested (PPH3 ≥ 0.99 throughout the discovery GWAS, Supp Table 9).

Gene to function

To understand putative biological mechanisms behind the potentially causal genes (*TBX15*, *WARS2*, *EBF2*), gene to function mapping was performed within FUMA. A visual representation of normalized gene expression across tissue types is depicted in **Supplementary Figure 8**, highlighting elevated expression of *EBF2* and *TBX15* in adipose tissue; with only *EBF2* specifically expressed in visceral omental adipose tissue. Differentially expressed gene set (DEG) analyses did not identify any statistically significant differences in gene expression across tissue types (**Supp Table 10**). The gene-set enrichment and pathway analyses did not yield any significant results.

A phenome-wide association study was performed for protein-coding potentially causal genes. The two prioritized genes on Chromosome 1, *TBX15* and *WARS2*, were associated with similar phenotypes, including male pattern baldness, white blood cells, measures of overall adiposity and its distribution, bone mineral density and height (**Supplementary Figure 9, Supp Table 11**). The prioritized Chromosome 8 gene, *EBF2*, was associated with traits relating to adiposity and its distribution and height, but was also associated with blood pressure traits. An association was also noted with inguinal hernias. The results are presented in **Supplementary Figure 10** and **Supp Table 11**. In mice, homozygous loss of function in both *EBF2* and *WARS2* have been associated with embryonic lethality, whereas heterozygous loss of function mutations in *EBF2* have been associated with a variety of cardiac, spleen, vascular and other malformations. The full list of mouse phenotypes is reported in **Supp Table 12.**

Heritability and phenotypic associations

Heritability and genetic correlations

The genome-wide heritability (h^2_g SNP) of adiposity-adjusted PAT was estimated at 9.15% (standard error 2.49%). The genetic correlations of adjusted PAT are displayed in **Supp**

Table 13. There was no significant correlation with adiposity measures; which is expected given the adjustment for these measures in the GWAS analysis. A nominally significant correlation was noted between adjusted PAT and heart failure (rG=0.36, se=0.18, p=0.048). No further correlations were discovered with other cardiovascular outcomes, and no associations were significant after accounting for multiple testing.

Mendelian randomization

The instrumental variants extracted for Mendelian randomization (MR) analyses corresponded with the two prioritized lead variants at the two risk loci. F-statistics were 34.5 for rs6428792, and 50.3 for rs11992444, indicating adequate instrument strength.

Higher genetically-predicted adjusted PAT was associated with lower LVEDV (β -1.04, 95%CI -1.88 to -0.19, p=0.016) and LVESV (β -0.91, 95%CI -1.74 to -0.08, p=0.032). There was no significant association between genetically-predicted PAT and LVSV (β -0.72, 95%CI -1.73 to 0.07, p=0.072), LVEF (β 0.23, 95%CI -0.64 to 1.11, p=0.602) and LVM/LVEDV Ratio (β 1.14, 95%CI -0.28 to 2.55, p=0.115).

The results of the MR analyses are summarized in **Figure 5** and **Supp Table 14**. Single SNP analysis revealed consistency in effect estimate directions with the main analysis and between both instrumental variants, as depicted in **Figure 6**.

Sensitivity analyses

The meta-analysis GWAS resulted in 185 SNPs that passed the GWAS p-value threshold (5×10^{-8}) mostly in chromosome 1 and 2 and one in chromosome 8 (Table 3). The leading SNPs are rs6428792 (Chr 1), rs1430788 (Chr 2) and rs1199244 (Chr 8) that are matching the GWAS summary of discovery and replication. rs1430788 (Chr 2) was neither significant in the discovery nor in the replication GWAS while it is among the leading SNPs in the meta analysis.

The results of the more relaxed GWAS (without adjustment for fat measures) are presented in **Supp Table 15**. rs11992444 (Chr 8) SNP that was replicated in the adjusted model and in the

meta analysis was also significant in the relaxed GWAS. In addition, the rs143078898 (Chr 2) SNP that was significant in the meta analysis GWAS was also significant in the relaxed GWAS analysis.

Discussion

This study is the largest individual-level GWAS to date exploring the polygenic basis and genetic architecture of PAT. To add to previous literature, we specifically aimed to disentangle PAT from multiple other biometric measures of total adiposity and its distribution, in order to isolate specific determinants of preferential fat deposition in the pericardial compartment. This strategy yielded a total of 11 genome-wide significant variants, with two lead uncorrelated SNPs relating to two genomic risk loci. These were mapped to ten potentially causal genes using positional, eQTL and chromatin interaction mapping. Among these, three protein coding genes were identified: *TBX15*, *WARS2*, and *EBF2*. For the latter two genes, enrichment analyses determined significant tissue-specific eQTLs and chromatin interactions in both adipose and cardiac tissue, supporting an overlapping physiology in these tissue types. Importantly, we also found that the proportion of phenotypic variance explained by the genotype was 9.1%, indicating a relatively high genetic determination of proportionally greater PAT deposition.

To date, only two genome-wide association studies[18,19] have been performed exploring the polygenic basis of PAT. Fox *et al*[48] explored the genetic determinants of PAT adjusted for visceral fat volume, WHR and BMI in 5,487 participants of the Framingham Heart Study, uncovering one single genome-wide significant variant at one locus (rs10198628 mapped to the *TRIB2* gene). In our relaxed GWAS, this SNP was only nominally associated with PAT (p-value = 0.029). The result was similar in the main GWAS analysis adjusted for fat measures (p-value= 0.037) and in the meta-analysis. (p-value= 0.012). Chu *et al*[18] explored the genetic determinants of PAT, adjusted for height and weight only, in a cohort of 18,332 participants that included individuals in Fox *et al*'s study. Three genome-wide significant variants were identified (rs6587515 mapped to the *ENSA* gene, rs1650505 mapped to the

EBF1 gene, and rs10198628 mapped to the *TRIB2* gene). Among them, one was replicated from Fox et al's study (rs10198628 (Chr 2)). In our 'relaxed' GWAS, rs6689335 was (p=0.320), rs6587515 was (p=0.220), and rs10198628 was (p=0.015). In the main GWAS analysis with adjustment for fat measures, rs6689335 was not associated with PAT (p=0.900) and neither was rs6587515 (p=0.150), whereas rs10198628 was (p=0.160). In the meta-analysis, rs6689335 (p=0.657) and rs6587515 (p=0.383) were not associated with PAT while rs10198628 (p=0.011) was nominally significant but did not pass GWAS threshold. This discrepancy is likely to relate to the lack of sample overlap, and more comprehensive adjustment for measures of total and relative adipose tissue distribution. Importantly, in our present study a replication analysis was carried out in an independent subset of UK Biobank participants that were excluded from the discovery analysis. This replicated all the genome-wide significant signals at Bonferroni-adjusted p-value, increasing confidence in the validity of the results.

Among the genome-wide significant variants discovered, ten of the eleven were located in a single genomic risk locus on Chromosome 1. Among these, one single lead variant was retained (rs6428792). Positional mapping identified three potential causal genes, eQTL mapping identified four potential causal genes (two overlapping) and chromatin interaction using Hi-C data from the left ventricle identified two further potential causal genes. Colocalisation analysis suggested that, for all the genes in the implicated region in chromosome 1, risk of PAT in both subcutaneous adipose and tibial arterial regions were associated with increase gene expression of RP4-712E4.1, a long non-coding RNA, at this locus. For the Chromosome 8 variant (rs11992444), positional and eQTL mapping did not identify any genes, and the colocalisation analysis was inconclusive. However, chromatin interaction mapping using Hi-C data from the left ventricle identified three potentially causal genes. Overall, among the identified potentially causal genes at both loci, five had been previously associated with BMI-adjusted adiposity distribution traits (*TBX15*, *WARS2*, *EBF2*,

444 *PSMC1P12*, *RNA5SP56*), and one gene, *SDAD1P1*, has been previously associated with red
445 cell distribution width. The remaining four genes had no previously reported associations.

446 The potentially causal protein-coding genes have been implicated in a variety of physiological
447 pathways. *EBF2* is known to play a key role in activating the expression of brown fat-
448 selective genes in adipocytes[55]. *WARS2* encodes a cytoplasmic form of tryptophanyl-tRNA
449 synthetase, which has been shown to play a central role in angiogenesis, including cardiac
450 angiogenesis[56]. In mouse models, reduction of *WARS2* gene function was shown to lead to
451 reduced food intake and depot-specific changes in fat mass and brown fat distribution[57].
452 Similarly, *TBX15* activation has been implicated in the preferential distribution of abdominal
453 adiposity[58] as well as in andergenic-induced adipocyte browning[59]. Generally, white adipose
454 tissue is considered predominantly an inactive energy storage, whereas brown adipose tissue
455 contains a higher concentration of mitochondria and expresses uncoupling protein 1 (UCP1),
456 a protein that enables its metabolic utilization and thermogenesis[60]. PAT is considered
457 predominantly a white adipose tissue depot, though it is known to have higher expression of
458 UCP1 compared to white adipose tissue in the rest of the body. The results of our study and
459 functional annotation suggest that a reduced propensity toward fat browning likely
460 contributes to higher proportional PAT deposition. Indeed, both lead variants in this study
461 were inversely associated with PAT, and unaligned eQTL mapping displayed a
462 predominantly inhibitory role of the unaligned variants on *WARS2*, but an enhancing role on
463 *TBX15*. Thus, aligning the variants towards greater PAT would suggest an enhancing role on
464 *WARS2*, and an inhibitory action on *TBX15*, both of which are consistent with a phenotype of
465 inhibited adipose tissue browning. This is mechanistically consistent with previous
466 observational work outlining an inverse association between brown adipose tissue and
467 visceral adiposity deposition[61].

468 To relate the genetic data with potential biological consequences of PAT, we examined
469 genetic correlation analyses and performed MR. A genetic correlation was observed between
470 adjusted PAT and HF, consistent with previous evidence linking PAT with heart failure[6] and

adverse cardiac structure and function independent of overall adiposity[9]. Building on this observational data, we performed MR analyses to elucidate the potential causal relevance of PAT on cardiac structure and function. This revealed an association of higher PAT with lower LVEDV, LVESV, and a suggestive result for lower LVSV. This is broadly reflective of a reduction in ventricular chamber volume, consistent with remodeling patterns seen in ageing[62] and in heart failure with a preserved ejection fraction (HFpEF)[63]. Beyond the reduction in left ventricular volumes and stroke volume, the ageing HFpEF phenotype is characterized by lower LV mass due to cardiomyocyte attrition[63,64], typically occurring to a lesser proportion to the reduction in volumes, leading to an increased LVM/LVEDV ratio reflecting greater concentricity[63]. In this phenotype, LVEF would be expected to remain similar, or paradoxically increase with the rise in concentricity[65]. Though not all these associations were statistically significant, the directionality of MR results is consistent with remodeling in a HFpEF cardiac phenotype. This is consistent with the cardiac remodeling pattern that has previously been associated with PAT in observational studies[66–68].

We acknowledge some limitations. Despite being the largest currently available GWAS of PAT, the number of loci discovered remains small. Additionally, due to the restricted sample size, analysis was restricted to variants with MAF>1%. Incorporation of rare variants in further analyses when larger sample sizes are available might enhance genetic discovery. Finally, the UK Biobank population was restricted to European ancestry, therefore further research is warranted in populations of other ancestries.

In summary, the results of this study enhance the current knowledge regarding the genetic basis of preferential PAT deposition, prioritized a number of potentially causal genes that might exert influence through modulation of adipose tissue browning, and provide genetic evidence to support causal relevance of PAT on cardiac structure and function that might contribute to heart failure risk.

References

1. Barandier C, Montani J-P, Yang Z. Mature adipocytes and perivascular adipose tissue stimulate vascular smooth muscle cell proliferation: effects of aging and obesity. *Am J Physiol Circ Physiol* 2005;**289**:H1807–H1813.

2. Henrichot E, Juge-Aubry CE, Pernin A, Pache J-C, Velebit V, Dayer J-M, Meda P, Chizzolini C, Meier CA. Production of Chemokines by Perivascular Adipose Tissue. *Arterioscler Thromb Vasc Biol* 2005;**25**:2594–2599.

3. Mazurek T, Zhang L, Zalewski A, Mannion JD, Diehl JT, Arafat H, Sarov-Blat L, O'Brien S, Keiper EA, Johnson AG, Martin J, Goldstein BJ, Shi Y. Human Epicardial Adipose Tissue Is a Source of Inflammatory Mediators. *Circulation* 2003;**108**:2460–2466.

4. Iacobellis G, Bianco AC. Epicardial adipose tissue: Emerging physiological, pathophysiological and clinical features. *Trends Endocrinol Metab* 2011;**22**:450–457.

5. Greif M, Becker A, Ziegler F Von, Lebherz C, Lehrke M, Broedl UC, Tittus J, Parhofer K, Becker C, Reiser M, Knez A, Leber AW. Pericardial Adipose Tissue Determined by Dual Source CT Is a Risk Factor for Coronary Atherosclerosis. *Arterioscler Thromb Vasc Biol* 2009;**29**:781–786.

6. Kenchaiah S, Ding J, Carr JJ, Allison MA, Budoff MJ, Tracy RP, Burke GL, McClelland RL, Arai AE, Bluemke DA. Pericardial Fat and the Risk of Heart Failure. *J Am Coll Cardiol* Elsevier Inc.; 2021;**77**:2638–2652.

7. Wong CX, Ganesan AN, Selvanayagam JB. Epicardial fat and atrial fibrillation: Current evidence, potential mechanisms, clinical implications, and future directions. Eur. Heart J. 2017.

8. Batal O, Schoenhagen P, Shao M, Ayyad AE, Wagoner DR Van, Halliburton SS, Tchou PJ, Chung MK. Left Atrial epicardial adiposity and Atrial fibrillation. *Circ Arrhythmia Electrophysiol* 2010;**3**:230–236.

9. Ardissino M, McCracken C, Bard A, Antoniades C, Neubauer S, Harvey NC, Petersen SE, Raisi-Estabragh Z. Pericardial adiposity is independently linked to adverse cardiovascular phenotypes: a CMR study of 42 598 UK Biobank participants. *Eur Hear J - Cardiovasc Imaging* 2022;**23**:1471–1481.

10. Shah R V., Anderson A, Ding J, Budoff M, Rider O, Petersen SE, Jensen MK, Koch M, Allison M, Kawel-Boehm N, Wisocky J, Jerosch-Herold M, Mukamal K, Lima JAC, Murthy VL. Pericardial, But Not Hepatic, Fat by CT Is Associated With CV Outcomes and Structure. *JACC Cardiovasc Imaging* 2017;**10**:1016–1027.

11. Rose KM, Newman B, Mayer-Davis EJ, Selby J V. Genetic and behavioral determinants of waist-hip ratio and waist circumference in women twins. *Obes Res* 1998;**6**:383–392.

12. Shungin D, Winkler TW, Croteau-Chonka DC, Ferreira T, Locke AE, Mägi R, Strawbridge RJ, Pers TH, Fischer K, Justice AE, Workalemahu T, Wu JMW, Buchkovich ML, Heard-Costa NL, Roman TS, Drong AW, Song C, Gustafsson S, Day FR, Esko T, Fall T, Kutalik Z, Luan J, Randall JC, Scherag A, Vedantam S, Wood AR, Chen J, Fehrmann R, Karjalainen J, et al. New genetic loci link adipose and insulin biology to body fat distribution. *Nature* 2015;**518**:187–196.

13. Pulit SL, Stoneman C, Morris AP, Wood AR, Glastonbury CA, Tyrrell J, Yengo L, Ferreira T, Marouli E, Ji Y, Yang J, Jones S, Beaumont R, Croteau-Chonka DC, Winkler TW, Hattersley AT, Loos RJF, Hirschhorn JN, Visscher PM, Frayling TM, Yaghootkar H, Lindgren CM. Meta-analysis of genome-wide association studies for body fat distribution in 694 649 individuals of European ancestry. *Hum Mol Genet* 2019;**28**:166–174.

14. Kaess BM, Pedley A, Massaro JM, Murabito J, Hoffmann U, Fox CS. The ratio of visceral to subcutaneous fat, a metric of body fat distribution, is a unique correlate of cardiometabolic risk. *Diabetologia* 2012;**55**:2622–2630.

15. Rosenquist KJ, Pedley A, Massaro JM, Therkelsen KE, Murabito JM, Hoffmann U, Fox CS. Visceral and Subcutaneous Fat Quality and Cardiometabolic Risk. *JACC Cardiovasc Imaging* 2013;**6**:762–771.

16. Britton KA, Massaro JM, Murabito JM, Kreger BE, Hoffmann U, Fox CS. Body Fat Distribution, Incident Cardiovascular Disease, Cancer, and All-Cause Mortality. *J Am Coll Cardiol* 2013;**62**:921–925.

17. Emdin CA, Khera A V, Natarajan P, Klarin D, Zekavat SM, Hsiao AJ, Kathiresan S. Genetic Association of Waist-to-Hip Ratio With Cardiometabolic Traits, Type 2 Diabetes, and Coronary Heart Disease. *JAMA* 2017;**317**:626–634.

18. Fox CS, White CC, Lohman K, Heard-Costa N, Cohen P, Zhang Y, Johnson AD, Emilsson V, Liu C-T, Chen Y-DI, Taylor KD, Allison M, Budoff M, Rotter JI, Carr JJ, Hoffmann U, Ding J, Cupples LA, Liu Y. Genome-Wide Association of Pericardial Fat Identifies a Unique Locus for Ectopic Fat. Snyder M, ed. *PLoS Genet* 2012;**8**:e1002705.

19. Chu AY, Deng X, Fisher VA, Drong A, Zhang Y, Feitosa MF, Liu C-T, Weeks O, Choh AC, Duan Q, Dyer TD, Eicher JD, Guo X, Heard-Costa NL, Kacprowski T, Kent JW, Lange LA, Liu X, Lohman K, Lu L, Mahajan A, O'Connell JR, Parihar A, Peralta JM, Smith A V, Zhang Y, Homuth G, Kissebah AH, Kullberg J, Laqua R, et al. Multiethnic genome-wide meta-analysis of ectopic fat depots identifies loci associated with adipocyte development and differentiation. *Nat Genet* 2017;**49**:125–130.

20. Bard A, Raisi-Estabragh Z, Ardissino M, Lee AM, Pugliese F, Dey D, Sarkar S, Munroe PB, Neubauer S, Harvey NC, Petersen SE. Automated Quality-Controlled Cardiovascular Magnetic Resonance Pericardial Fat Quantification Using a Convolutional Neural Network in the UK Biobank. *Front Cardiovasc Med* 2021;**8**:1–11.

21. UK Biobank: Protocol for a large-scale prospective epidemiological resource. 2007.

22. Petersen SE, Matthews PM, Francis JM, Robson MD, Zemrak F, Boubertakh R, Young AA, Hudson S, Weale P, Garratt S, Collins R, Piechnik S, Neubauer S. UK Biobank's cardiovascular magnetic resonance protocol. *J Cardiovasc Magn Reson* BioMed Central; 2015;**18**:8.

23. UK Biobank. Body Composition Measurement.

24. West J, Leinhard OD, Romu T, Collins R, Garratt S, Bell JD, Borga M, Thomas L. Feasibility of MR-based body composition analysis In large scale population studies. *PLoS One* 2016;**11**:1–14.

25. Purcell S, Neale B, Todd-Brown K, Thomas L, Ferreira MAR, Bender D, Maller J, Sklar P, Bakker PIW de, Daly MJ, Sham PC. PLINK: a tool set for whole-genome association and population-based linkage analyses. *Am J Hum Genet* 2007;**81**:559–575.

26. Loh P-R, Tucker G, Bulik-Sullivan BK, Vilhjálmsson BJ, Finucane HK, Salem RM, Chasman DI, Ridker PM, Neale BM, Berger B, Patterson N, Price AL. Efficient Bayesian mixed-model analysis increases association power in large cohorts. *Nat Genet* 2015;**47**:284–290.

27. Willer CJ, Li Y, Abecasis GR. METAL: fast and efficient meta-analysis of genomewide association scans. *Bioinformatics* 2010;**26**:2190–2191.

28. Watanabe K, Taskesen E, Bochoven A van, Posthuma D. Functional mapping and annotation of genetic associations with FUMA. *Nat Commun* 2017;**8**:1826.

29. 1000 Genomes Project Consortium, Auton A, Brooks LD, Durbin RM, Garrison EP, Kang HM, Korbel JO, Marchini JL, McCarthy S, McVean GA, Abecasis GR. A global reference for human genetic variation. *Nature* 2015;**526**:68–74.

30. Buniello A, Macarthur JAL, Cerezo M, Harris LW, Hayhurst J, Malangone C,

McMahon A, Morales J, Mountjoy E, Sollis E, Suveges D, Vrousgou O, Whetzel PL, Amode R, Guillen JA, Riat HS, Trevanion SJ, Hall P, Junkins H, Flicek P, Burdett T, Hindorff LA, Cunningham F, Parkinson H. The NHGRI-EBI GWAS Catalog of published genome-wide association studies, targeted arrays and summary statistics 2019. *Nucleic Acids Res* 2019;

31. Wang K, Li M, Hakonarson H. ANNOVAR: functional annotation of genetic variants from high-throughput sequencing data. *Nucleic Acids Res* 2010;**38**:e164.

32. Kircher M, Witten DM, Jain P, O'Roak BJ, Cooper GM, Shendure J. A general framework for estimating the relative pathogenicity of human genetic variants. *Nat Genet* 2014;**46**:310–315.

33. Boyle AP, Hong EL, Hariharan M, Cheng Y, Schaub MA, Kasowski M, Karczewski KJ, Park J, Hitz BC, Weng S, Cherry JM, Snyder M. Annotation of functional variation in personal genomes using RegulomeDB. *Genome Res* 2012;**22**:1790–1797.

34. Roadmap Epigenomics Consortium, Kundaje A, Meuleman W, Ernst J, Bilenky M, Yen A, Heravi-Moussavi A, Kheradpour P, Zhang Z, Wang J, Ziller MJ, Amin V, Whitaker JW, Schultz MD, Ward LD, Sarkar A, Quon G, Sandstrom RS, Eaton ML, Wu Y-C, Pfenning AR, Wang X, Claussnitzer M, Liu Y, Coarfa C, Harris RA, Shoresh N, Epstein CB, Gjoneska E, Leung D, et al. Integrative analysis of 111 reference human epigenomes. *Nature* 2015;**518**:317–330.

35. Ernst J, Kellis M. ChromHMM: automating chromatin-state discovery and characterization. *Nat Methods* 2012;**9**:215–216.

36. GTEx Consortium, Laboratory DA &Coordinating C (LDACC)—Analysis WG, Statistical Methods groups—Analysis Working Group, Enhancing GTEx (eGTEx) groups, NIH Common Fund, NIH/NCI, NIH/NHGRI, NIH/NIMH, NIH/NIDA, Biospecimen Collection Source Site—NDRI, Biospecimen Collection Source Site—RPCI, Biospecimen Core Resource—VARI, Brain Bank Repository—University of

Miami Brain Endowment Bank, Leidos Biomedical—Project Management, ELSI Study, Genome Browser Data Integration &Visualization—EBI, Genome Browser Data Integration &Visualization—UCSC Genomics Institute U of CSC, Lead analysts:, Laboratory DA &Coordinating C (LDACC):, NIH program management:, Biospecimen collection:, Pathology:, eQTL manuscript working group:, Battle A, Brown CD, Engelhardt BE, Montgomery SB. Genetic effects on gene expression across human tissues. *Nature* 2017;**550**:204–213.

37. Wang D, Liu S, Warrell J, Won H, Shi X, Navarro FCP, Clarke D, Gu M, Emani P, Yang YT, Xu M, Gandal MJ, Lou S, Zhang J, Park JJ, Yan C, Rhie SK, Manakongtreecheep K, Zhou H, Nathan A, Peters M, Mattei E, Fitzgerald D, Brunetti T, Moore J, Jiang Y, Girdhar K, Hoffman GE, Kalayci S, Gümüş ZH, et al. Comprehensive functional genomic resource and integrative model for the human brain. *Science (80-)* 2018;**362**.

38. Lek M, Karczewski KJ, Minikel E V, Samocha KE, Banks E, Fennell T, O'Donnell-Luria AH, Ware JS, Hill AJ, Cummings BB, Tukiainen T, Birnbaum DP, Kosmicki JA, Duncan LE, Estrada K, Zhao F, Zou J, Pierce-Hoffman E, Berghout J, Cooper DN, Deflaux N, DePristo M, Do R, Flannick J, Fromer M, Gauthier L, Goldstein J, Gupta N, Howrigan D, Kiezun A, et al. Analysis of protein-coding genetic variation in 60,706 humans. *Nature* 2016;**536**:285–291.

39. Petrovski S, Gussow AB, Wang Q, Halvorsen M, Han Y, Weir WH, Allen AS, Goldstein DB. The Intolerance of Regulatory Sequence to Genetic Variation Predicts Gene Dosage Sensitivity. *PLoS Genet* 2015;**11**:e1005492.

40. Leeuw CA de, Mooij JM, Heskes T, Posthuma D. MAGMA: Generalized Gene-Set Analysis of GWAS Data. Tang H, ed. *PLOS Comput Biol* 2015;**11**:e1004219.

41. Wijst MGP van der, Brugge H, Vries DH de, Deelen P, Swertz MA, LifeLines Cohort Study, BIOS Consortium, Franke L. Single-cell RNA sequencing identifies celltype-

specific cis-eQTLs and co-expression QTLs. *Nat Genet* 2018;**50**:493–497.

42. Schmitt AD, Hu M, Jung I, Xu Z, Qiu Y, Tan CL, Li Y, Lin S, Lin Y, Barr CL, Ren B. A Compendium of Chromatin Contact Maps Reveals Spatially Active Regions in the Human Genome. *Cell Rep* 2016;**17**:2042–2059.

43. Lizio M, Harshbarger J, Shimoji H, Severin J, Kasukawa T, Sahin S, Abugessaisa I, Fukuda S, Hori F, Ishikawa-Kato S, Mungall CJ, Arner E, Baillie JK, Bertin N, Bono H, Hoon M de, Diehl AD, Dimont E, Freeman TC, Fujieda K, Hide W, Kaliyaperumal R, Katayama T, Lassmann T, Meehan TF, Nishikata K, Ono H, Rehli M, Sandelin A, Schultes EA, et al. Gateways to the FANTOM5 promoter level mammalian expression atlas. *Genome Biol* 2015;**16**:22.

44. Lu L, Liu X, Huang W-K, Giusti-Rodríguez P, Cui J, Zhang S, Xu W, Wen Z, Ma S, Rosen JD, Xu Z, Bartels CF, Kawaguchi R, Hu M, Scacheri PC, Rong Z, Li Y, Sullivan PF, Song H, Ming G, Li Y, Jin F. Robust Hi-C Maps of Enhancer-Promoter Interactions Reveal the Function of Non-coding Genome in Neural Development and Diseases. *Mol Cell* 2020;**79**:521-534.e15.

45. Watanabe K, Stringer S, Frei O, Umićević Mirkov M, Leeuw C de, Polderman TJC, Sluis S van der, Andreassen OA, Neale BM, Posthuma D. A global overview of pleiotropy and genetic architecture in complex traits. *Nat Genet* 2019;**51**:1339–1348.

46. Groza T, Gomez FL, Mashhadi HH, Muñoz-Fuentes V, Gunes O, Wilson R, Cacheiro P, Frost A, Keskivali-Bond P, Vardal B, McCoy A, Cheng TK, Santos L, Wells S, Smedley D, Mallon A-M, Parkinson H. The International Mouse Phenotyping Consortium: comprehensive knockout phenotyping underpinning the study of human disease. *Nucleic Acids Res* 2022;

47. Giambartolomei C, Vukcevic D, Schadt EE, Franke L, Hingorani AD, Wallace C, Plagnol V. Bayesian Test for Colocalisation between Pairs of Genetic Association Studies Using Summary Statistics. *PLoS Genet* 2014;**10**.

48. Wallace C. Eliciting priors and relaxing the single causal variant assumption in colocalisation analyses. Epstein MP, ed. *PLOS Genet* 2020;**16**:e1008720.

49. Lonsdale J, Thomas J, Salvatore M, Phillips R, Lo E, Shad S, Hasz R, Walters G, Garcia F, Young N, Foster B, Moser M, Karasik E, Gillard B, Ramsey K, Sullivan S, Bridge J, Magazine H, Syron J, Fleming J, Siminoff L, Traino H, Mosavel M, Barker L, Jewell S, Rohrer D, Maxim D, Filkins D, Harbach P, Cortadillo E, et al. The Genotype-Tissue Expression (GTEx) project. *Nat Genet* 2013;**45**:580–585.

50. Pirruccello JP, Achille P Di, Nauffal V, Nekoui M, Friedman SF, Klarqvist MDR, Chaffin MD, Weng L-C, Cunningham JW, Khurshid S, Roselli C, Lin H, Koyama S, Ito K, Kamatani Y, Komuro I, BioBank Japan Project, Jurgens SJ, Benjamin EJ, Batra P, Natarajan P, Ng K, Hoffmann U, Lubitz SA, Ho JE, Lindsay ME, Philippakis AA, Ellinor PT. Genetic analysis of right heart structure and function in 40,000 people. *Nat Genet* 2022;**54**:792–803.

51. Aung N, Vargas JD, Yang C, Cabrera CP, Warren HR, Fung K, Tzanis E, Barnes MR, Rotter JI, Taylor KD, Manichaikul AW, Lima JAC, Bluemke DA, Piechnik SK, Neubauer S, Munroe PB, Petersen SE. Genome-wide analysis of left ventricular image-derived phenotypes identifies fourteen loci associated with cardiac morphogenesis and heart failure development. *Circulation* 2019;**140**:1318–1330.

52. Minelli C, Greco M. F Del, Plaat DA van der, Bowden J, Sheehan NA, Thompson J. The use of two-sample methods for Mendelian randomization analyses on single large datasets. *Int J Epidemiol* 2021;**50**:1651–1659.

53. Yavorska OO, Burgess S. MendelianRandomization: an R package for performing Mendelian randomization analyses using summarized data. *Int J Epidemiol* 2017;**46**:1734–1739.

54. R Core Team. R: A language and environment for statistical computing. *R Found Stat Comput Vienna, Austria URL https//wwwR-project.org/* 2022;

55. Shapira SN, Lim H-W, Rajakumari S, Sakers AP, Ishibashi J, Harms MJ, Won K-J, Seale P. EBF2 transcriptionally regulates brown adipogenesis via the histone reader DPF3 and the BAF chromatin remodeling complex. *Genes Dev* 2017;**31**:660–673.

56. Wang M, Sips P, Khin E, Rotival M, Sun X, Ahmed R, Widjaja AA, Schafer S, Yusoff P, Choksi PK, Ko NSJ, Singh MK, Epstein D, Guan Y, Houštěk J, Mracek T, Nuskova H, Mikell B, Tan J, Pesce F, Kolar F, Bottolo L, Mancini M, Hubner N, Pravenec M, Petretto E, MacRae C, Cook SA. Wars2 is a determinant of angiogenesis. *Nat Commun* 2016;**7**:12061.

57. Mušo M, Bentley L, Vizor L, Yon M, Burling K, Barker P, Zolkiewski LAK, Cox RD, Dumbell R. A Wars2 mutant mouse shows a sex and diet specific change in fat distribution, reduced food intake and depot-specific upregulation of WAT browning. *Front Physiol* 2022;**13**.

58. Pan DZ, Miao Z, Comenho C, Rajkumar S, Koka A, Lee SHT, Alvarez M, Kaminska D, Ko A, Sinsheimer JS, Mohlke KL, Mancuso N, Muñoz-Hernandez LL, Herrera-Hernandez M, Tusié-Luna MT, Aguilar-Salinas C, Pietiläinen KH, Pihlajamäki J, Laakso M, Garske KM, Pajukanta P. Identification of TBX15 as an adipose master trans regulator of abdominal obesity genes. *Genome Med* 2021;**13**:123.

59. Sun W, Zhao X, Wang Z, Chu Y, Mao L, Lin S, Gao X, Song Y, Hui X, Jia S, Tang S, Xu Y, Xu A, Loomes K, Wang C, Wu D, Nie T. Tbx15 is required for adipocyte browning induced by adrenergic signaling pathway. *Mol Metab* 2019;**28**:48–57.

60. Townsend K, Tseng Y-H. Brown adipose tissue: Recent insights into development, metabolic function and therapeutic potential. *Adipocyte* 2012;**1**:13–24.

61. Wibmer AG, Becher T, Eljalby M, Crane A, Andrieu PC, Jiang CS, Vaughan R, Schöder H, Cohen P. Brown adipose tissue is associated with healthier body fat distribution and metabolic benefits independent of regional adiposity. *Cell Reports Med* 2021;**2**:100332.

62. Cheng S, Fernandes VRS, Bluemke DA, McClelland RL, Kronmal RA, Lima JAC. Age-Related Left Ventricular Remodeling and Associated Risk for Cardiovascular Outcomes. *Circ Cardiovasc Imaging* 2009;**2**:191–198.

63. Samson R, Jaiswal A, Ennezat P V., Cassidy M, Jemtel TH Le. Clinical Phenotypes in Heart Failure With Preserved Ejection Fraction. *J Am Heart Assoc* 2016;**5**.

64. Anversa P, Hiler B, Ricci R, Guideri G, Olivetti G. Myocyte cell loss and myocyte hypertrophy in the aging rat heart. *J Am Coll Cardiol* 1986;**8**:1441–1448.

65. Shah S, Segar MW, Kondamudi N, Ayers C, Chandra A, Matulevicius S, Agusala K, Peshock R, Abbara S, Michos ED, Drazner MH, Lima JAC, Longstreth WT, Pandey A. Supranormal Left Ventricular Ejection Fraction, Stroke Volume, and Cardiovascular Risk. *JACC Hear Fail* 2022;**10**:583–594.

66. Woerden G van, Gorter TM, Westenbrink BD, Willems TP, Veldhuisen DJ van, Rienstra M. Epicardial fat in heart failure patients with mid-range and preserved ejection fraction. *Eur J Heart Fail* John Wiley and Sons Ltd; 2018;**20**:1559–1566.

67. Mahabadi AA, Anapliotis V, Dykun I, Hendricks S, Al-Rashid F, Lüdike P, Totzeck M, Rassaf T. Epicardial fat and incident heart failure with preserved ejection fraction in patients with coronary artery disease. *Int J Cardiol* 2022;

68. Kenchaiah S, Ding J, Carr JJ, Allison MA, Budoff MJ, Tracy RP, Burke GL, McClelland RL, Arai AE, Bluemke DA. Pericardial Fat and the Risk of Heart Failure. *J Am Coll Cardiol* 2021;**77**:2638–2652.

.

Acknowledgements

Disclosures

Conflicts of interest

SEP provides Consultancy to Circle Cardiovascular Imaging Inc., Calgary, Alberta, Canada.

Funding

AS is supported by a British Heart Foundation project grant (PG/21/10619).

MA is funded by a National Institute for Health and Care Research for an Academic Clinical Fellowship.

Barts Charity (G-002346) contributed to fees required to access UK Biobank data [access application #2964]. SEP acknowledges the British Heart Foundation for funding the manual analysis to create a cardiovascular magnetic resonance imaging reference standard for the UK Biobank imaging resource in 5000 CMR scans (www.bhf.org.uk; PG/14/89/31194).

Z.R.E. was supported by British Heart Foundation Clinical Research Training Fellowship No. FS/17/81/33318.

SEP acknowledges support from the National Institute for Health and Care Research (NIHR) Biomedical Research Centre at Barts.

S.E.P. and L.S. have received funding from the European Union's Horizon 2020 research and innovation programme under grant agreement No 825903 (euCanSHare project).

SEP acknowledges support from and from the "SmartHeart" EPSRC programme grant (www.nihr.ac.uk; EP/P001009/1).

This article is supported by the London Medical Imaging and Artificial Intelligence Centre for Value Based Healthcare (AI4VBH), which is funded from the Data to Early Diagnosis and Precision Medicine strand of the government's Industrial Strategy Challenge Fund, managed and delivered by Innovate UK on behalf of UK Research and Innovation (UKRI).

Views expressed are those of the authors and not necessarily those of the AI4VBH Consortium members, the NHS, Innovate UK, or UKRI.

This work was supported by Health Data Research UK, an initiative funded by UK Research and Innovation, Department of Health and Social Care (England) and the devolved administrations, and leading medical research charities.

The funders provided support in the form of salaries for authors as detailed above, but did not have any additional role in the study design, data collection and analysis, decision to publish, or preparation of the manuscript.

.

Figure Legends

Figure 1 – Methods and key results of functional annotation of genome-wide significant variants, and exploration of functional consequences of prioritised variants and genes.

Figure 2 – Regional plot of the Chromosome 1 locus. Genes prioritized by FUMA are highlighted in red, and genome-wide significant SNPs are coloured based on r^2. From the top; genome-wide significance p-value, CADD score and eQTL P-value. eQTLs are plotted for each gene and are colored based on tissue types.

Figure 3 – Chromatin interactions and eQTLs of PAT risk loci on Chr1. The outer layer displays GWAS p-values, with the lead SNP labelled. Genes mapped by either eQTLs or chromatin interactions are displayed in the innermost circle. Genes mapped by chromatin interactions are displayed in orange, eQTLs in green, and those mapped by both red. Orange links display chromatin interactions, green links display eQTLs.

Figure 4 – Chromatin interactions and eQTLs of PAT risk loci on Chr8. The outer layer displays GWAS p-values, with the lead SNP labelled. Genes mapped by either eQTLs or chromatin interactions are displayed in the innermost circle. Genes mapped by chromatin interactions are displayed in orange, eQTLs in green, and those mapped by both red. Orange links display chromatin interactions, green links display eQTLs.

Figure 5 – Inverse-variance weighted Mendelian randomization analysis exploring the association between pericardial fat area (PAT) and left ventricular end diastolic volume (LVEDV), end systolic volume (LVESV), ejection fraction (LVEF), mass (LVM) and mass to end diastolic volume ratio (LVM:LVEDV).

Figure 6 – Single-SNP Mendelian randomization analysis (Wald ratio method) exploring the association between pericardial fat area (PAT) through rs6428792 and rs11992444; and left ventricular end diastolic volume (LVEDV), end systolic volume (LVESV), ejection fraction (LVEF), mass (LVM) and mass to end diastolic volume ratio (LVM:LVEDV).

Supplementary Figure 1 – Genome-wide significant variants for pericardial fat area after adjusting for sex, age, age^2, age*sex, 10 genetic principal components (PCs), assessment centre, genotype array, and 2 PCs reflecting BMI, WHR, whole body fat mass, trunk fat mass, body fat percentage. The dashed line represents the genome-wide significance threshold, $p<5x10^{-8}$.

Supplementary Figure 2 – Q-Q plot of for association of genetic variants with pericardial fat area after adjusting for sex, age, age^2, age*sex, 10 genetic principal components (PCs), assessment centre, genotype array, and 2 PCs reflecting BMI, WHR, whole body fat mass, trunk fat mass, body fat percentage. The dashed line represents the null hypothesis.

Supplementary Figure 3 – Manhattan plot of the MAGMA gene-based test. The red line represents genome wide significance. With the inclusion of 19,086 protein coding genes, this was defined at $P = 0.05/19086 = 2.62x10^{-6}$

Supplementary Figure 4 – Results from colocalisation analysis of RP4-712E4.1 in subcetaneous adipose tissue. A and C show regional association plots for Regional association plots for GWAS and eQTL respectively, with chromosome position as mapped in GRCh38. Comparison of betas (B), and p-values (D) from eQTLs and GWAS are shown, with overlay of Pearson's correlation)

Supplementary Figure 5 – Results from colocalisation analysis of RP4-712E4.1 in tibial artery. A and C show regional association plots for regional association plots for GWAS and eQTL respectively, with chromosome position as mapped in GRCh38. Comparison of betas (B), and p-values (D) from eQTLs and GWAS are shown, with overlay of Pearson's correlation).

Supplementary Figure 6. Results of sensitivity analysis showing prior and posterior probability distributions as a function of the p_{12} prior for: A – RP4-712E4.1 in subcutaneous adipose tissue; B – RP4-712E4.1 in tibial artery; and C – CDCA2 in the left ventricle.

Supplementary Figure 7. Results from colocalisation analysis of CDCA2 in the left ventricle. A and C show regional association plots for regional association plots for GWAS and eQTL respectively, with chromosome position as mapped in GRCh38. Comparison of betas (B), and p-values (D) from eQTLs and GWAS are shown, with overlay of Pearson's correlation). Results are driven by a single SNP and are therefore less likely to be a true colocalisation.

Supplementary Figure 8 – Average normalised expression of all mapped genes in 54 tissue types extracted from GTEx v8. Red indicates higher gene expression, normalised per gene.

Supplementary Figure 9 – Phenome-wide associations for TBX15 and WARS2 gene among currently available studies on GWASAtlas. Coloring corresponds to phenotype cluster, summarized in labels on the right. Only associations with a minimum p-value of 0.05 are displayed.

Supplementary Figure 10 – Phenome-wide associations for EBF2 gene among currently available studies on GWASAtlas. Coloring corresponds to phenotype cluster, summarized in labels on the right. Only associations with a minimum p-value of 0.05 are displayed.

Tables

Table 1 – Genome-wide significant variants. Genome-wide analysis identified 11 sentinel variants that were genome-wide significant ($P<5x10^{-8}$). The table displays beta coefficients with standard errors, and p-value estimates. Allele 1 is the effect allele.

SNP	Chrom	Pos	Allele 1	Allele 0	Allele 1 Frequency	Missing rate	Beta	Std error	p-value
rs11992444	8	25464690	G	T	0.490	0.003	-0.012	0.002	1.30E-12
rs6428792	1	119656867	G	A	0.380	0.006	-0.010	0.002	4.20E-09
rs10923752	1	119658925	G	A	0.341	0.007	0.010	0.002	1.40E-08
rs10923748	1	119647946	G	C	0.341	0.007	0.010	0.002	1.60E-08
rs6428794	1	119657743	A	T	0.341	0.007	0.010	0.002	1.60E-08
rs12036872	1	119660505	C	G	0.341	0.007	0.010	0.002	1.60E-08
rs4304634	1	119650931	T	A	0.340	0.009	0.010	0.002	1.80E-08
rs764891110	1	119651167	T	TTATGA	0.341	0.010	0.010	0.002	1.80E-08

rs4659150	1	119660819	T	G	0.340	0.008	0.010	0.002	1.90E-08
rs4659146	1	119645535	T	C	0.342	0.009	0.010	0.002	2.10E-08
rs2885227	1	119650928	C	A	0.340	0.009	0.010	0.002	2.00E-08

Table 2 – Replication of association between genome-wide significant variants and adjusted pericardial fat area (PAT) in the testing set. All variants passed replication at Bonferroni-adjusted statistical significance threshold ($P<4.5x10^{-3}$).

SNP	**Chrom**	**Pos**	**Allele 1**	**Allele 0**	**Allele 1 Frequency**	**Missing rate**	**Beta**	**Std error**	**p-value**
rs11992444	8	25464690	G	T	0.489	0.002	-0.015	0.002	5.00E-11
rs6428792	1	119656867	G	A	0.380	0.007	-0.008	0.002	0.00078
rs10923752	1	119658925	G	A	0.339	0.008	0.007	0.002	0.0028
rs10923748	1	119647946	G	C	0.339	0.008	0.007	0.002	0.0026
rs6428794	1	119657743	A	T	0.339	0.008	0.007	0.002	0.0027
rs12036872	1	119660505	C	G	0.339	0.008	0.007	0.002	0.0027
rs4304634	1	119650931	T	A	0.338	0.009	0.007	0.002	0.0026
rs764891110	1	119651167	T	TTATGA	0.339	0.011	0.007	0.002	0.0025

rs4659150	1	119660819	T	G	0.338	0.008	0.007	0.002	0.0026
rs4659146	1	119645535	T	C	0.339	0.010	0.007	0.002	0.0021
rs2885227	1	119650928	C	A	0.338	0.009	0.007	0.002	0.0025

Table 3 – Meta-analysis GWAS summary statistics for the lead SNPs using the Metal tool.

SNP	CHR	BP	Allele1	Allele2	Effect	StdErr	P-value	Direction
rs6428792	1	119656867	A	G	-0.0092	0.0014	1.67E-11	--
rs143078898	2	229994086	T	C	-0.0133	0.0023	1.53E-08	--
rs11992444	8	25464690	T	G	-0.0127	0.0013	8.77E-22	--

Supplemental tables Legends

Supplementary Table 1 – Candidate SNPs, defined as all genome-wide significant SNPs associated with adjusted PAT ($p<5x10^{-8}$) and additional highly correlated SNPs identified via 1000G Phase 3 data.

Supplementary Table 2 – Genomic risk loci of interest, respective lead SNPs and independent significant SNPs in the locus.

Supplementary Table 3 – Lead SNPs identified from genome-wide SNPs at $r^2<0.1$. Genomic locus: the index of genomic risk loci specified in Supp Tab 3. #Ind. Sig. SNPs: Independent significant SNPs which are in LD with the corresponding lead SNPs at $r^2<0.1$

Supplementary Table 4 – Phenotypic associations for lead SNPs and additional closely correlated SNPs ($r^2>0.8$) available in GWASCatalog

Supplementary Table 5 – Variant annotation for all candidate SNPs using ANNOVAR.

Supplementary Table 6 – Genes prioritized using positional mapping, eQTL mapping (immune cells, arterial, adipose and cardiac tissue types) and chromatin interaction (aorta, right ventricle, left ventricle) mapping.

Supplementary Table 7 –Tissue-specific eQTLs discovered in adipose, heart and arterial tissue for genomic risk loci (FDR<0.05).

Supplementary Table 8 – Significant chromatin interactions (Hi-C) within aorta, left ventricle and right ventricle discovered for genomic risk loci (FDR<0.05).

Supplementary Table 9 – Results for colocalisation analysis. Table shows results for all genes within 1Mb of a significant GWAS hit, tested with expression quatitative trait loci from GTEx8. PPH4 > 0.8 suggests colocalisation of GWAS risk and gene expression. Abbreviations: nsnps – number of snps tested at a locus; PP.H0-4.abf – posterior probability of hypothesis 0-4 respectively; sum_PPH3_PPH4 - sum of posterior hypotheses 3 and 4; ratio_PPH4_PPH3 – ratio of posterior hypothesis 4 to posterior hypothesis 3.

Supplementary Table 10 – Differential gene expression analysis (DEG) comparing expression of candidate genes in each tissue type, versus all other tissue types.

Supplementary Table 11– Phenome-wide associations for EBF2, TBX15 and WARS2 gene among currently available studies on GWASAtlas.

Supplementary Table 12 – List of prior associations for loss-of-function in potential causal genes with phenotypes in mouse studies, sources using International Mouse Phenotyping Consortium (IMPC) data.

Supplementary Table 13 – Genetic correlations between PAT and adiposity traits (trunk fat mass ad percentage, whole body fat mass), cardiovascular risk factors (hypertension, diabetes, obesity), and cardiovascular outcomes (coronary heart disease, coronary event, heart failure, stroke, atrial fibrillation and flutter, and cardiac death).

Supplementary Table 14 – Mendelian randomization analysis exploring the association between genetically-predicted pericardial fat area (PAT), overall and in single-SNP analysis, and left ventricular end diastolic volume (LVEDV), end systolic volume (LVESV), stroke volume (LVSV), ejection fraction (LVEF), mass (LVM) and mass to end diastolic volume ratio (LVM/LVEDV Ratio).

Supplementary Table 15 – Genome-wide significant variants without adjustment for fat measures. The table displays beta coefficients with standard errors, and p-value estimates. Allele 1 is the effect allele.

Functional mapping

Genome-wide association study results

Age, sex, BMI, WHR, whole body fat mass, trunk fat mass and body fat percentage-adjusted **pericardial fat area**

Characterizing genomic loci

1. Independent significant SNPs + candidates in LD
2. Definition of genomic loci
3. Definition of lead SNPs

→

Characterizing genomic loci

3 independent significant SNPs ($p<5x10^{-8}$, $r^2<0.6$)
2 risk loci (Chr1:119645535-119742942, Chr8:25464690)
2 lead SNPs (rs6428792 and rs11992444, at $r^2<0.1$)

Annotating candidate SNPs

1. Functional consequences on genes (ANNOVAR)
2. Genome-wide gene-based analysis (MAGMA)
3. Deleteriousness (CADD)
4. Regulatory functions (RegulomeDB)
5. 15-core chromatin state
6. eQTL (GTEx V8)
7. Previous phenotypic associations (GWASCatalog)

→

Gene mapping

1. Positional mapping
2. eQTL mapping (adipose, cardiac, arterial tissues)
3. Chromatin interaction mapping (aortic, left and right ventricular tissues)

Gene mapping

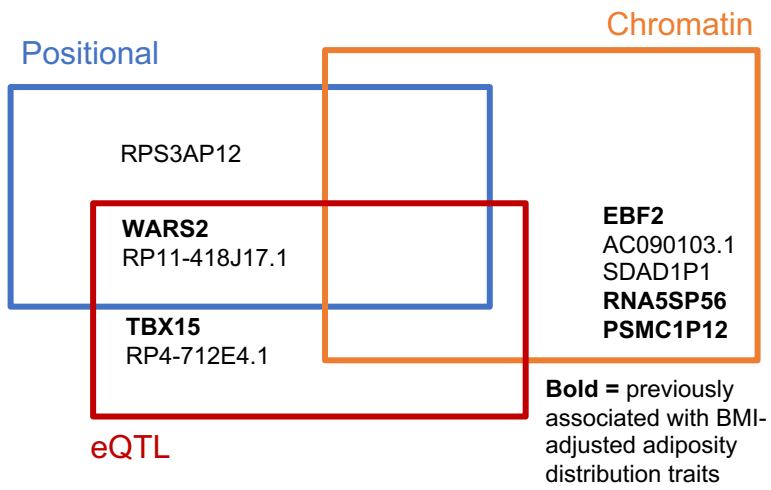

Gene to function

1. Normalized gene expression heatmap
2. Tissue specificity (DEG analysis)
3. Phenome-wide association study (OpenGWAS)
4. Previous mouse model associations (IPMC)
5. Mendelian randomization for causal relevance on cardiac structure and function

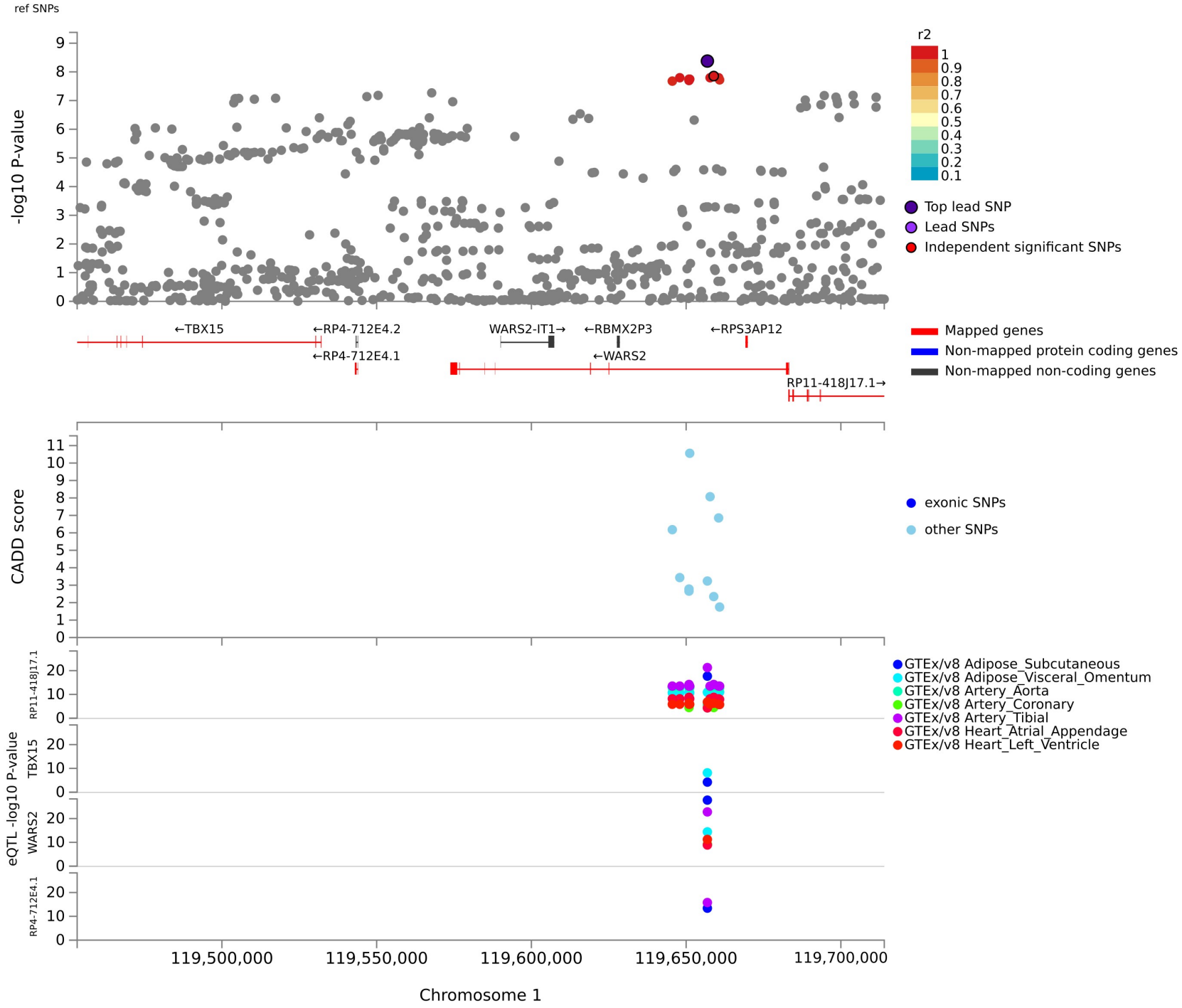
ref SNPs
-log10 P-value
r2
1
0.9
0.8
0.7
0.6
0.5
0.4
0.3
0.2
0.1
Top lead SNP
Lead SNPs
Independent significant SNPs
←TBX15
←RP4-712E4.2
←RP4-712E4.1
WARS2-IT1→
←RBMX2P3
←WARS2
←RPS3AP12
RP11-418J17.1→
Mapped genes
Non-mapped protein coding genes
Non-mapped non-coding genes
CADD score
exonic SNPs
other SNPs
eQTL -log10 P-value
RP11-418J17.1
TBX15
WARS2
RP4-712E4.1
GTEx/v8 Adipose_Subcutaneous
GTEx/v8 Adipose_Visceral_Omentum
GTEx/v8 Artery_Aorta
GTEx/v8 Artery_Coronary
GTEx/v8 Artery_Tibial
GTEx/v8 Heart_Atrial_Appendage
GTEx/v8 Heart_Left_Ventricle
119,500,000
119,550,000
119,600,000
119,650,000
119,700,000
Chromosome 1

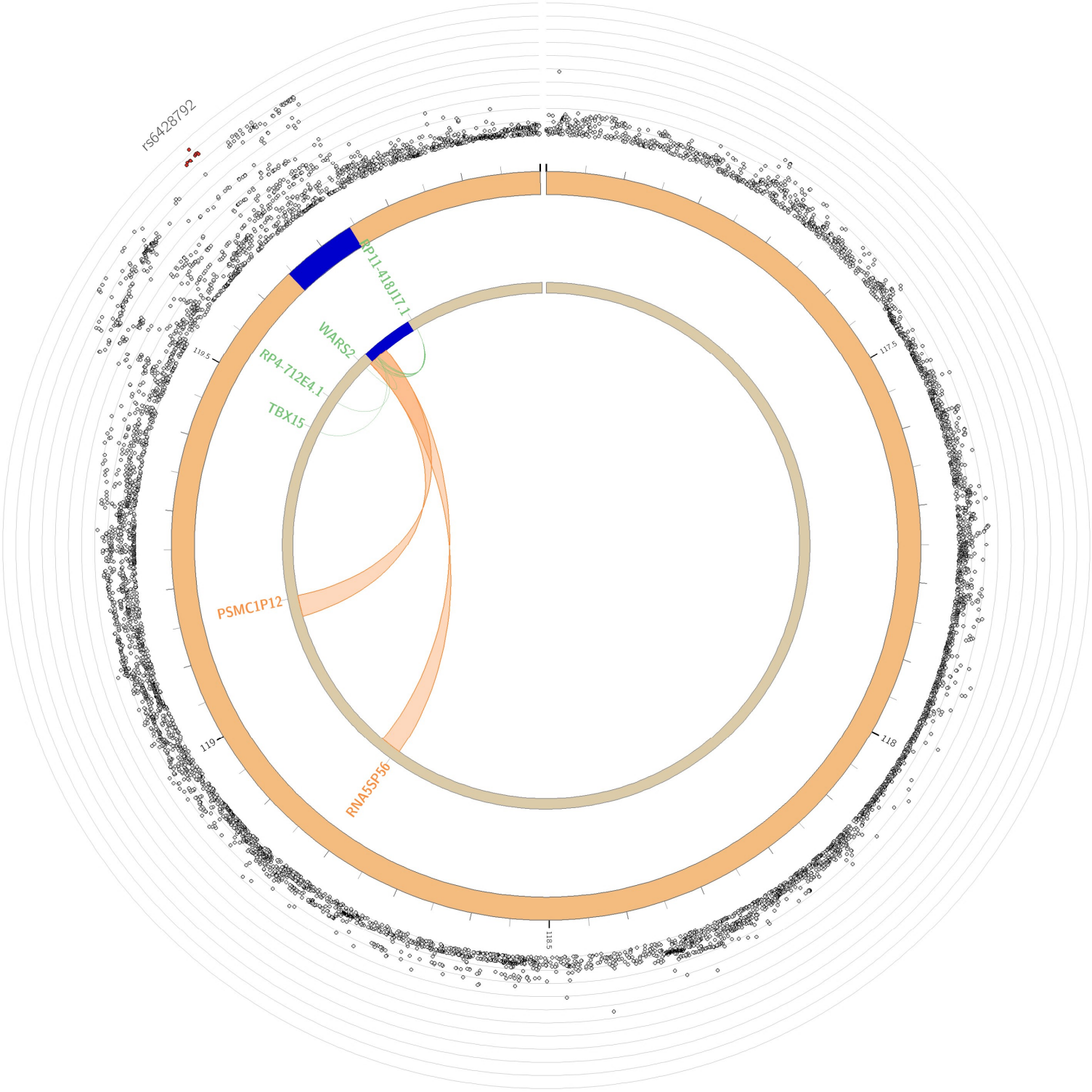
rs6428792
RP11-418J17.1
WARS2
RP4-712E4.1
TBX15
PSMC1P12
RNA5SP56
119.5
119
118.5
117.5
118


SDAD1P1
EBF2
AC090103.1
26.5
24.5
26
25
25.5
rs11992444

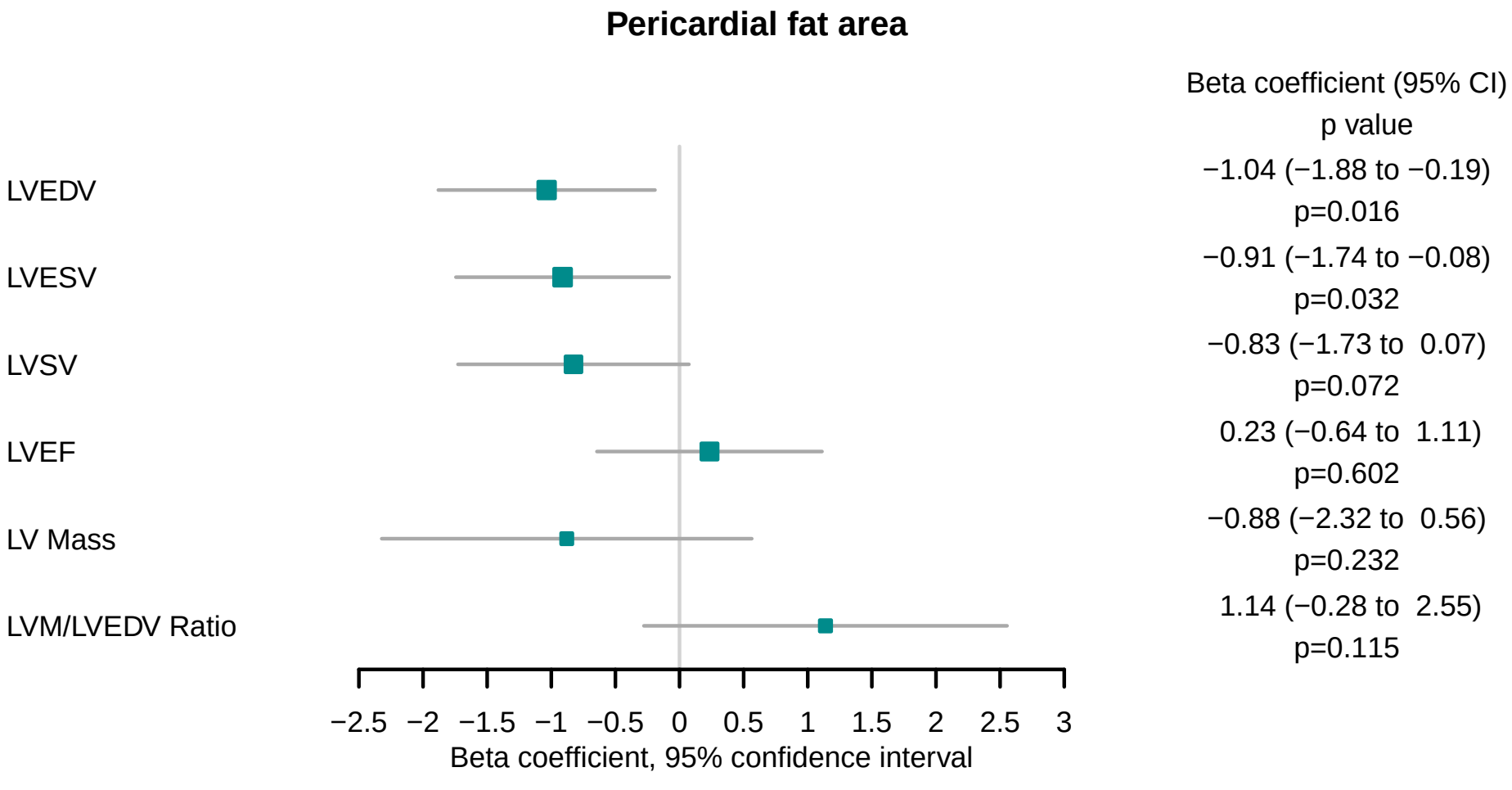
Pericardial fat area
Beta coefficient (95% CI)
p value
LVEDV
LVESV
LVSV
LVEF
LV Mass
LVM/LVEDV Ratio
−1.04 (−1.88 to −0.19)
p=0.016
−0.91 (−1.74 to −0.08)
p=0.032
−0.83 (−1.73 to 0.07)
p=0.072
0.23 (−0.64 to 1.11)
p=0.602
−0.88 (−2.32 to 0.56)
p=0.232
1.14 (−0.28 to 2.55)
p=0.115
−2.5 −2 −1.5 −1 −0.5 0 0.5 1 1.5 2 2.5 3
Beta coefficient, 95% confidence interval

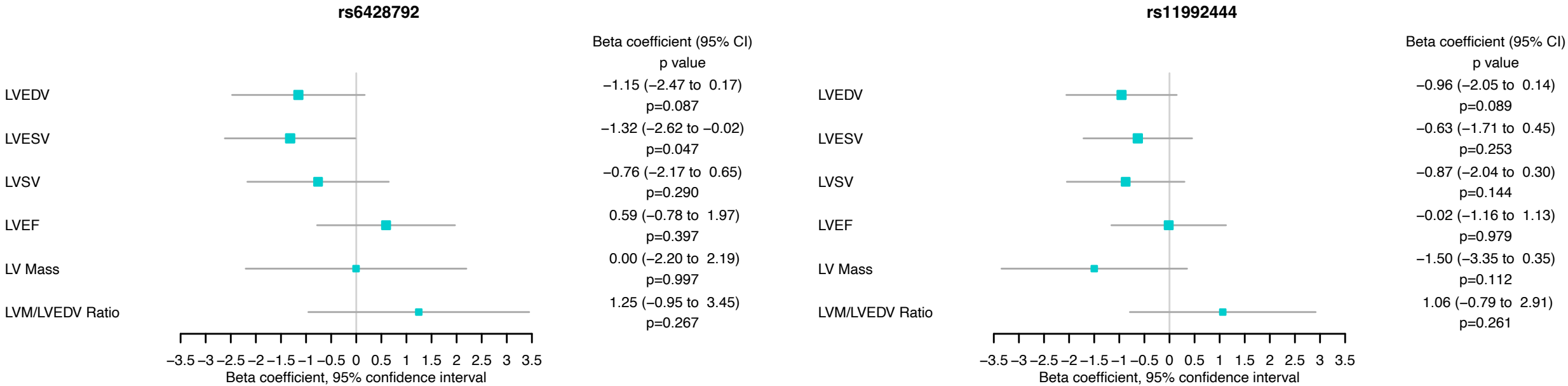
rs6428792
Beta coefficient (95% CI)
p value
LVEDV
−1.15 (−2.47 to 0.17)
p=0.087
LVESV
−1.32 (−2.62 to −0.02)
p=0.047
LVSV
−0.76 (−2.17 to 0.65)
p=0.290
LVEF
0.59 (−0.78 to 1.97)
p=0.397
LV Mass
0.00 (−2.20 to 2.19)
p=0.997
LVM/LVEDV Ratio
1.25 (−0.95 to 3.45)
p=0.267
−3.5 −3 −2.5 −2 −1.5 −1 −0.5 0 0.5 1 1.5 2 2.5 3 3.5
Beta coefficient, 95% confidence interval
rs11992444
Beta coefficient (95% CI)
p value
LVEDV
−0.96 (−2.05 to 0.14)
p=0.089
LVESV
−0.63 (−1.71 to 0.45)
p=0.253
LVSV
−0.87 (−2.04 to 0.30)
p=0.144
LVEF
−0.02 (−1.16 to 1.13)
p=0.979
LV Mass
−1.50 (−3.35 to 0.35)
p=0.112
LVM/LVEDV Ratio
1.06 (−0.79 to 2.91)
p=0.261
−3.5 −3 −2.5 −2 −1.5 −1 −0.5 0 0.5 1 1.5 2 2.5 3 3.5
Beta coefficient, 95% confidence interval